Influence of surface losses and the self-pumping effect on current-voltage characteristics of a long Josephson junction

A. L. Pankratov*
Institute for Physics of Microstructures of RAS, Nizhny Novgorod, 603950 Russia

A. S. Sobolev† and V. P. Koshelets‡
Institute of Radio Engineering and Electronics, Moscow, 125009 Russia

J. Mygind§
Department of Physics, Technical University of Denmark, Kongens Lyngby, DK–2800 Denmark
(Received 14 November 2006; revised manuscript received 22 March 2007; published 18 May 2007)

We have numerically investigated the dynamics of a long linear Josephson tunnel junction with overlap geometry. Biased by a direct current (dc) and an applied dc magnetic field, the junction has important applications as tunable high frequency oscillator [flux-flow oscillator (FFO)] in the millimeter and submillimeter range. The study is performed in the frame of a modified sine-Gordon model, which includes surface losses, self-pumping effect, and in an empirical way the superconducting gap. The electromagnetic coupling to the environment is modeled by a simple resistor-capacitor load (*RC* load) placed at both ends of the FFO. In our model, the damping parameter depends both on the spatial coordinate and on the amplitude of the ac voltage. In order to find the dc current-voltage curves, the damping parameter has to be calculated self-consistently by successive approximations and time integration of the perturbed sine-Gordon equation. The modified model gives better qualitative agreement with experimental results than the conventional perturbed sine-Gordon model.

DOI: 10.1103/PhysRevB.75.184516 PACS number(s): 74.50.+r, 85.25.Hv, 85.25.Cp, 74.40.+k

I. INTRODUCTION

During the past decade, the flux-flow oscillator[1] (FFO) has been considered as the most promising local oscillator in superconducting integrated submillimeter receivers[2] and spectrometers for space-born radio astronomy and atmosphere monitoring due to its wide operational bandwidth, easy broadband tunability, and relatively high radiation power. The FFO is a long linear Josephson junction in which a viscous flow of magnetic-flux quanta (fluxons) is maintained by a dc bias current and an applied dc magnetic field. The spectral linewidth of the radiation emitted from the ends of the free-running FFO is important for its ability to be frequency and phase locked. Typically, the observed free-running linewidth is 2–20 MHz for Nb-AlO_x-Nb FFO in the 400–700 GHz frequency range. The dynamical and fluctuational properties of the FFO have been intensively studied both experimentally and theoretically.[1–20] In contrast to many other types of oscillators, the FFO fluctuations are mainly caused by *internal* wideband sources, such as thermal and shot noise, that result in a spectral line of emission with nearly perfect Lorentzian shape. The power in the so-called "wings" decreases much slower with frequency offset from the carrier than the Gaussian shaped spectral line obtained when *external* noise sources are dominant. Thus, for the FFO, most external noise sources can be neglected since they, on one hand, are masked by the internal wideband fluctuations and, on the other hand, can be compensated by frequency locking to reference oscillators or high-Q cavities. It is a pertinent fundamental and technical problem to reduce the free-running linewidth of the FFO.

In order to make an optimal FFO design, which satisfies the technical requirements for practical applications, we need a trustable mathematical model that includes both high- and low-frequency effects. However, previous theoretical attempts to reproduce the detailed behavior of the dc current-voltage characteristics (IVCs) of practical FFOs were not fully successful: with given parameters, one could either reproduce the steep Fiske steps or the fairly smooth flux-flow curve. The characteristic structure observed at the so-called boundary voltage due to the self-pumping effect has only been studied by Koshelets *et al.*[7] In the present paper, we propose a modified sine-Gordon model which takes into account both surface losses and the self-pumping effect. Also, a simple resistor-capacitor load (*RC* load) is simulated at both ends of the FFO in order to model the electromagnetic coupling to the environment. Using the model we are able to calculate dc IVCs which are qualitatively similar to the experimental curves, and to explain some of their peculiarities.

II. MODEL

For several decades, the sine-Gordon model has been the most adequate model for the long Josephson junction, giving a good qualitative description of its basic properties, such as Fiske resonances, vortices dynamics, etc.:

$$\phi_{tt} + \alpha\phi_t - \phi_{xx} = \beta\phi_{xxt} + \eta(x) - \sin(\phi), \qquad (1)$$

where indices t and x denote temporal and spatial derivatives, respectively. Space and time have been normalized to the Josephson penetration length λ_J and to the inverse maximum plasma frequency ω_p^{-1}, respectively, α is the damping parameter, β is the surface loss parameter, and $\eta(x)$ is the normalized dc overlap bias current density. The proper value

of the surface loss parameter β is still unclear, but it definitely depends on voltage, so we started out from the value $\beta \approx 0.03$. Note that the bias current density is, as usual, normalized to the critical current density, and $\alpha = \omega_p/\omega_c$, where $\omega_p = \sqrt{2eI_c/\hbar C}$, $\omega_c = 2eI_cR_N/\hbar$, I_c is the critical current, C is the Josephson tunnel junction (JTJ) capacitance, and R_N is the normal-state resistance.

The boundary conditions, which are related to the external dc magnetic fields, the distribution of the dc bias current, and the high-frequency electromagnetic coupling to the environment are very important. In practice, the magnetic fields at the FFO ends used as boundary conditions for the one-dimensional (1D) sine-Gordon equation are created by the control line current running in the ground electrode along the junction. If the electrode's topology is not symmetric, the magnetic field will not be symmetric either, because it is determined by the geometry of the electrodes in the vicinity of the FFO ends. When the FFO is used as a local oscillator in practical microwave circuits, one needs to match its low impedance at the "radiating end" with the high impedance of an SIS mixer. The signal from the FFO is fed to the mixer via a microstrip line with some filtering elements. This network, connected to the radiating end ($x=0$ in our model), provides the situation when the FFO radiating end is well matched to the external environment, while the opposite end $x=L$ (where the chain of fluxons enters the junction) is strongly mismatched. Obviously, due to this reason, the magnetic-field values are not equal at the opposite FFO ends. These conditions were introduced into the model by choosing proper parameters of the *RC* loads and magnetic-field misbalance in the boundary conditions. So, we consider a JTJ of the so-called overlap geometry, where a small asymmetry of FFO is introduced as a small inline component of the current and use, therefore, the following boundary conditions (see Ref. 4):

$$\phi(0,t)_x + r_L c_L \phi(0,t)_{xt} - c_L \phi(0,t)_{tt} + \beta r_R c_R \phi(0,t)_{xtt} + \beta \phi(0,t)_{xt} = \Gamma - \Delta\Gamma \tag{2}$$

and

$$\phi(L,t)_x + r_R c_R \phi(L,t)_{xt} + c_R \phi(L,t)_{tt} + \beta r_R c_R \phi(L,t)_{xtt} + \beta \phi(L,t)_{xt} = \Gamma + \Delta\Gamma \tag{3}$$

that simulate simple *RC* loads. Γ is the normalized magnetic field, and $\Delta\Gamma = 0.05\Gamma$ is a small magnetic-field difference (introduced as an experimentally motivated fitting parameter, usually, $\Delta\Gamma$ is of the order of 5%–20%). The dimensionless capacitances and resistances, $c_{L,R}$ and $r_{L,R}$, are the FFO *RC* load placed at the left (output) and at the right (input) ends, respectively. It should be noted that, following Ref. 20, if both overlap $\eta_{ov} = \eta(x)$ and inline $\eta_{in} = 2\Delta\Gamma/L$ components of the current are present, the total current density, $\eta_t(x)$, with respect to which all current-voltage characteristics will be computed, is the sum of overlap and inline components: $\eta_t(x) = \eta(x) + 2\Delta\Gamma/L$. This is actually the same, see Ref. 21, as to consider the bias current $\eta(x)$ to be the total current, but then an additional term $-d\Gamma(x)/dx$ in the sine-Gordon equation should be taken into account that for linear dependence of $\Gamma(x)$ is just $-2\Delta\Gamma/L$, giving, therefore, the same current-voltage characteristic.

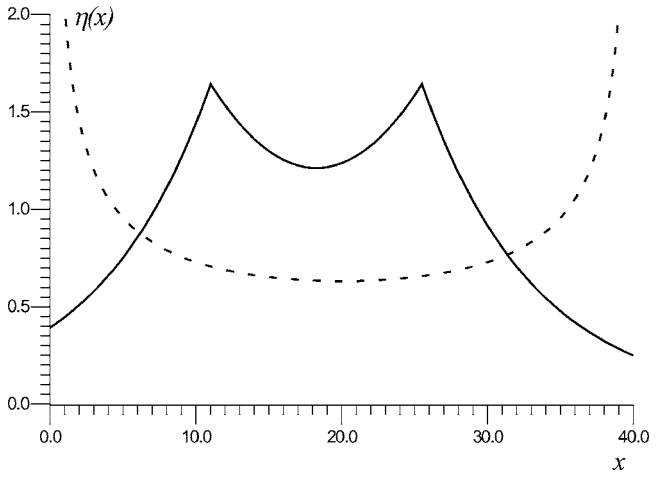

FIG. 1. The distribution of overlap component of bias current $\eta(x)$. Short-dashed line: $\eta(x) = \frac{\eta_0 L}{\pi\sqrt{x(L-x)}}$; solid curve: $x_0 = 11$, $x_1 = 25.5$, $p = 0.13$, and $a = 0.005$.

The profile of the dc bias current is not known and should be calculated from a three-dimensional (3D) model of the JTJ with a realistic geometry of the bias electrodes. From the experimental design, one can, however, make a qualified guess on the qualitative behavior of the overlap component of bias current profile, e.g., the positions of the two maxima for this function are located at the edges of the current injector electrode. As a few possible situations, let us consider the current profiles, depicted in Fig. 1. Since the JTJ is long compared to its width, one can use, as a first approximation, the current profile known for a superconducting film: $\eta(x) = \frac{\eta_0 L}{\pi\sqrt{x(L-x)}}$ (see, e.g., Ref. 22), where L is the dimensionless length of the JTJ and η_0 is a constant given by the total overlap component of the current in the film. In order to describe also the situation where the width of the bias electrodes is smaller than the junction length (as it was realized in some experimental designs), let us consider the current profile, depicted in Fig. 1 by the solid curve. Here, we assumed that the current profile is parabolic (with the curvature $a = 0.005$ in Fig. 1) between the left and the right boundaries of bias electrode x_0 and x_1 ($0 \leqslant x_0 \leqslant x \leqslant x_1 \leqslant L$) and drops down exponentially in the unbiased tails $x \leqslant x_0$, $x \geqslant x_1$ with the decay factor p: $\exp(-px)$ (with $p = 0.13$ in Fig. 1). The decay factor and the parabolic curvature will be used as fitting parameters when we make a comparison with the experimental IVCs.

III. INFLUENCE OF SURFACE LOSSES ON CURRENT-VOLTAGE CHARACTERISTICS

First, let us investigate the conventional sine-Gordon model including the surface losses term $\beta\phi_{xxt}$, as given by Eq. (1). To solve Eq. (1) numerically, we have used the implicit difference scheme described, e.g., in Ref. 23. If the model parameters are selected close to the experimental ones, the numerical simulations of Eq. (1) give a moderate

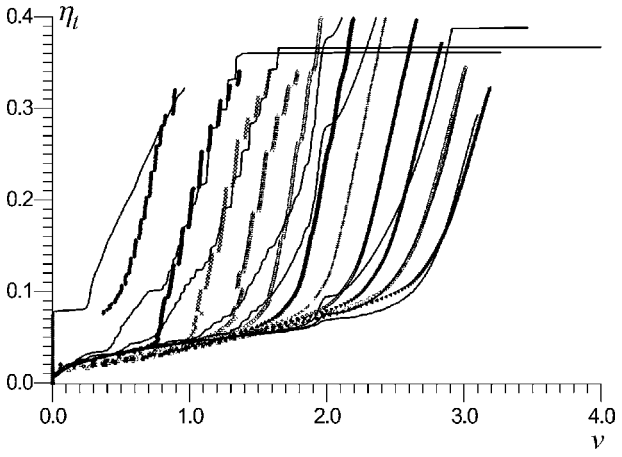

FIG. 2. A series of dc current-voltage characteristics each obtained for incremented values (from left to right $\Gamma = 1.85; 2.0; 2.2; \ldots; 3.6; 3.8$) of the external magnetic field for the following parameters: $L=40$, $\alpha=0.033$, $\beta=0.035$, $c_L=c_R=10$, $r_L=2$, and $r_R=100$. Thin lines: experimental measurements. Numerical simulations: triangles, crosses, circles, diamonds, etc., for the current profile depicted in Fig. 1 by the solid line.

qualitative agreement with the measured IVCs [i.e., the dependence of the time-averaged dimensionless voltage $v(t) = d\phi/dt$ on the total bias current $\eta_t = \eta_0 + 2\Delta\Gamma/L$, $\eta_0 = (1/L)\int_0^L \eta(x)dx$] (see Fig. 2). Namely, the JTJ length is $L=40$, $\alpha=0.033$, $\beta=0.035$, $c_L=c_R=10$, $r_L=2$, and $r_R=100$; and the polarity of the bias current and the magnetic field Γ are chosen such that the fluxon chain moves from right to left.

A typical set of experimental IVCs at different fixed values of the magnetic field for a Nb-AlO_x-Nb FFO is shown in Fig. 2 (thin solid lines). In this figure, the experimental data are represented in the space of normalized units valid for Eq. (1). In order to make unit conversion correctly, we need to know the total critical current I_c of the junction and ω_p, as the dc voltage has to be finally normalized to $\omega_p \hbar/2e$. We took $I_c = 0.72\delta Ig$ and $\omega_p = C_{SW}/\lambda_J$, where C_{SW} is the Swihart velocity and δIg is the jump of the quasiparticle current at the superconducting gap voltage v_g. In the experiment, these parameters had the following values: $I_c = 243$ mA and $\omega_p = 1.28 \times 10^{12}$ Hz. It gives the normalized value of v_g equal to 5.7. The so-called "boundary voltage," which is $1/3\ v_g$, clearly divides the family of IVCs into two regions with a boundary at $v_b = 1.9$. Below v_b, the IVC consists of nearly vertical, equally spaced voltage spikes, the so-called Fiske steps, which are due to electromagnetic resonances (Fiske resonances) in the JTJ. Above v_b, the damping parameter is drastically increased due to the so-called self-pumping effect,[7] which is explained as a resonant tunneling of quasiparticles similar to the well-known photon-assisted tunneling (PAT). As it was shown in Ref. 7 the self-pumping results in an increase of the quasiparticle current and accordingly the shunt damping α. This results in a broadening of the resonant Fiske steps and a transformation of the IVC into the smooth so-called flux-flow curve. For $v > v_b$, continuous tuning of the FFO frequency is possible and for fixed bias current, the junction dc voltage increases approximately proportional to the magnetic field.

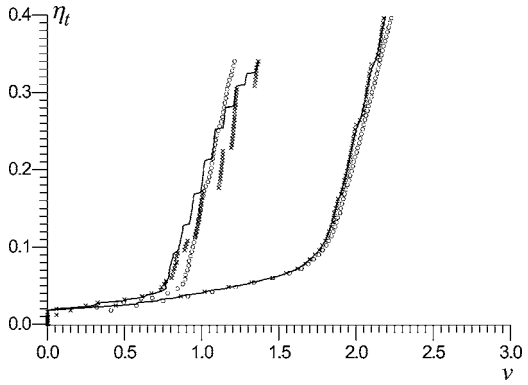

FIG. 3. Calculated current-voltage characteristics of the FFO. Numerical simulations for different values of the load; crosses, unloaded symmetrical case; thin lines, asymmetric load $r_L=2$, $r_R=100$; and circles, perfect matching $r_L=r_R=1$; all other parameters are the same as used for the IVCs in Fig. 2.

However, as it follows from Fig. 2, even without accounting for the self-pumping effect, but with the surface losses included, one can see the same IVC behavior: smoothing at higher oscillation frequency. It leads to a qualitative coincidence between the experimental and theoretical results for the bias current profile, depicted in Fig. 1 by the solid line. It is known that it is very difficult to numerically calculate the IVC for a long JTJ with small damping, i.e., in the region with steep Fiske steps (voltage spaced as π/L). Usually, the solution gets locked around one step and it is only possible to "jump" to neighboring steps by, e.g., changing the initial conditions. In the present case, however, all the Fiske steps could be calculated using a continuous change of bias current, probably due to the account of surface losses, which makes the curves smoother.

IV. INFLUENCE OF *RC* LOAD ON CURRENT-VOLTAGE CHARACTERISTICS

In Fig. 3, we have calculated the effect of the high-frequency load on the Fiske steps using the same parameters and current profile as for the IVCs shown in Fig. 2. Firstly, the almost unloaded symmetric case, $r_L=r_R=100$ (crosses in Fig. 3), the Fiske steps extend to higher currents and seem to have larger voltage spacing (sometimes even by the separation $2\pi/L$) when compared to the asymmetric case with $r_L=2$, $r_R=100$ (solid lines). Secondly, with a perfect match at both ends ($r_L=r_R=1$, circles), the Fiske steps disappear almost completely, see the curve for $\Gamma=2$. The same behavior is also observed for larger magnetic field $\Gamma=2.8$, the only difference being that the Fiske steps are smoother due to the surface losses.

V. INCLUDING THE SELF-PUMPING EFFECT

In order to give a better description of the experimental situation, one should incorporate into the sine-Gordon model the self-pumping effect, with α being defined self-consistently from the amplitude of the ac voltage. If we start from the unpumped dc IVC, $\eta_t(v_{dc})$, and apply a high-

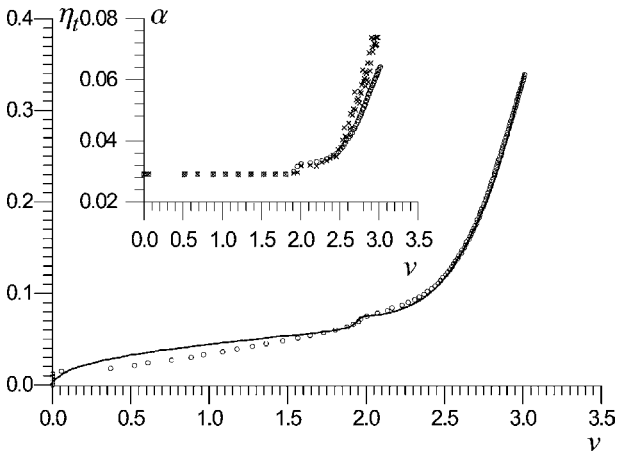

FIG. 4. Current-voltage characteristics of the FFO. Thin line—experimental measurements. Numerical simulations including the self-pumping effect—circles. Inset: the damping factor $\alpha(x)$ at the middle of the junction (crosses) and spatially averaged over x (circles).

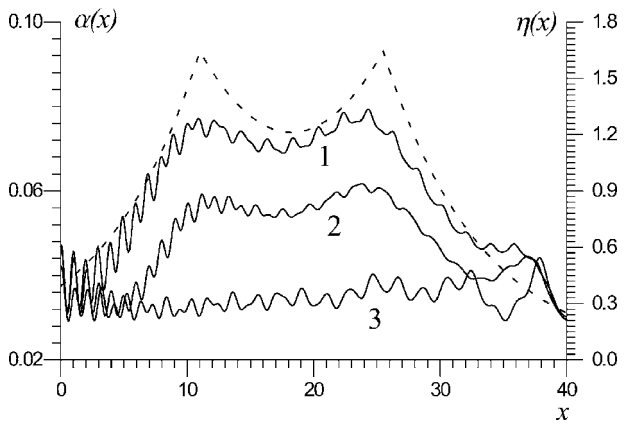

FIG. 5. Spatial dependence of the shunt damping $\alpha(x)$ for three currents η_t; $\Gamma=3.7$: curve 1, $\eta_t=0.3$; curve 2, $\eta_t=0.2$; and curve 3, $\eta_t=0.1$. The dashed line represents the distribution of $\eta(x)$.

frequency signal, so the total voltage across the junction is $v(t)=v_{dc}+v_{ac}\cos(\omega t+\psi)$, then, according to Ref. 24, the total dc quasiparticle tunneling current η_{pump} of the pumped junction will be given by

$$\eta_{pump}(v_{dc},\omega,v_{ac})=\sum_{n=-\infty}^{n=+\infty}J_n^2\left(\frac{ev_{ac}}{\hbar\omega}\right)\eta_t(v_{dc}+n\hbar\omega/e), \quad (4)$$

where J_n are the Bessel functions. One can use this formula for the PAT of quasiparticles to take into account the self-pumping effect by treating the Josephson radiation as an external signal. Therefore, if we take $v_{dc}=\hbar\omega/2e$ and the parameter α (which has to be dependent on the coordinate x) as the ratio η_{pump}/v_{dc}, we get $\alpha=\eta_{pump}(v_{ac}(x),x)/v_{dc}$. In our simulations, we took $\eta_t(v_{dc})$ of the unpumped FFO following the nonlinear resistive model as [see Ref. 25, formula (2.27)]

$$\eta_t=\alpha_0 v\left\{b\frac{(v/v_g)^n}{[(v/v_g)^n+1]}+1\right\}.$$

Here, the factor $b=R_j/R_n=35$ (compare with $b=R_j/R_n=25$ in Ref. 7) is the ratio between the normal-state resistances below and above the gap voltage. The power index n may be taken from 10 to ∞, while we took $n=80$; however, there were no visible differences between calculated curves for n ranging from 20 to 80.

With these modifications, the self-pumped IVC can be numerically computed using the iterative procedure combined with the implicit difference scheme for the solution of Eq. (1). Namely, at the first step, the ac voltage of JTJ with a certain initial value of α is calculated. At the second step, the obtained ac voltage $v_{ac}(x)$ is considered to pump the JTJ. Here, the damping $\alpha(x)=\eta_{pump}[v_{ac}(x),x]/v_{dc}$ is computed. This procedure is repeated with a new $\alpha(x)$ until the steady-state value of v_{dc} is found with a desired precision. The IVC obtained by this approach is shown in Fig. 4 (circles). It has a steplike peculiarity on the foot of the curves at the boundary voltage, similar to that observed for the experimentally measured *IV* curves [Fig. 4, thin lines, see also the same peculiarity for $\alpha(v)$ in the inset]. The curve is computed for almost the same parameters as in Fig. 2 and $\Gamma=3.7$, $L=40$, $\beta=0.04$, $c_L=c_R=10$, $r_L=2$, and $r_R=100$.

In spite of the nearly perfect coincidence of the numerically computed curve with the experimental curve, it should be noted that the formula [Eq. (4)] is valid only for small driving amplitudes, and the curves calculated for large self-pumping steps demonstrate unstable behavior. To extend our analysis for arbitrary values of the self-pumping steps, one should either use a more exact formula instead of Eq. (4) or even consider a more general integral equation instead of the sine-Gordon equation (1). Nevertheless, the presented approach allows us to perform the analysis of the self-pumping effect and, in particular, to study the dependence of Ohmic losses versus the dc voltage and the spatial coordinate x. The inset of Fig. 4 shows the damping $\alpha(x)$ in the middle of the junction (crosses) and averaged over the coordinate x (circles). The damping increases significantly (up to three times) for voltages above $v_b=1.9$ as predicted in Ref. 7. In difference with Ref. 7, in the inset of Fig. 4, α is considered in a large scale, so if one cuts the curves up to voltages 2.4, and consider in more detail the currents below 0.04, one will see the same qualitative behavior of α as in Ref. 7, with the only exception, we do not observe the small step at $v_g/5$, since we consider pumping the FFO by its own radiated signal, which is rather small for small currents/voltages, while in Ref. 7 this pumping is considered to be with a constant amplitude irrespectively to the junction's biasing point. The functions $\alpha(x)$ for the three total bias current values η_t (calculated for the corresponding voltages of Fig. 4) are shown in Fig. 5 together with the distribution of the applied bias current $\eta(x)$. It is seen that $\alpha(x)$ increases with increasing overlap bias current density $\eta(x)$, and this effect is even more pronounced for large voltages, where the self-pumping effect increases.

VI. CONCLUSIONS

The present paper contains an analysis of the nonlinear dynamics of a long overlap Josephson tunnel junction in the

frame of a modified sine-Gordon model which takes into account surface losses and *RC* load at both ends of the junction. It is demonstrated that the qualitative behavior of the dc current-voltage characteristics of a real flux-flow oscillator may be reproduced using a realistic set of junction and bias parameters. In particular, the transition from the *I-V* curve with steep and narrow voltage spaced Fiske steps to the smooth *I-V* curve in the flux-flow region may be explained by the joint influence of surface losses and self-pumping effect. It was shown that the self-pumping effect may increase the Ohmic losses up to three times, which in turn leads to additional smoothing of the *I-V* curves. The obtained results give us the hope that the use of more advanced models will allow for a very detailed prediction of the *I-V* characteristics of practical FFOs. Future work may include static calculations of bias current profiles in the frame of two-dimensional (2D) or 3D models and substitution of the calculated profiles into the 1D sine-Gordon model with more accurate account of the self-pumping effect, or even the use of full 2D and 3D dynamic models, where the bias current flow is calculated self-consistently.

ACKNOWLEDGMENTS

The authors wish to thank E. Goldobin for discussions. The work was supported by the RFBR Project No. 06-02-17206, ISTC Project No. 3174, NATO SfP Grant No. 981415, the President Grant for Leading Scientific School 7812.2006.2, CSTP Contract No. 02.442.11.7342, the Danish Natural Science Foundation, and the Hartmann Foundation.

*Electronic address: alp@ipm.sci-nnov.ru
†Electronic address: sobolev@hitech.cplire.ru
‡Electronic address: valery@hitech.cplire.ru
§Electronic address: myg@fysik.dtu.dk

[1] T. Nagatsuma, K. Enpuku, F. Irie, and K. Yoshida, J. Appl. Phys. **54**, 3302 (1983); see also **56**, 3284 (1984); **58**, 441 (1985); **63**, 1130 (1988).
[2] V. P. Koshelets and S. V. Shitov, Supercond. Sci. Technol. **13**, R53 (2000).
[3] V. P. Koshelets, A. Shchukin, I. L. Lapytskaya, and J. Mygind, Phys. Rev. B **51**, 6536 (1995).
[4] C. Soriano, G. Costabile, and R. D. Parmentier, Supercond. Sci. Technol. **9**, 578 (1996).
[5] A. A. Golubov, B. A. Malomed, and A. V. Ustinov, Phys. Rev. B **54**, 3047 (1996).
[6] A. V. Ustinov, H. Kohlstedt, and P. Henne, Phys. Rev. Lett. **77**, 3617 (1996).
[7] V. P. Koshelets, S. V. Shitov, A. V. Shchukin, L. V. Filippenko, J. Mygind, and A. V. Ustinov, Phys. Rev. B **56**, 5572 (1997).
[8] A. P. Betenev and V. V. Kurin, Phys. Rev. B **56**, 7855 (1997).
[9] M. Cirillo, N. Grønbech-Jensen, M. R. Samuelsen, M. Salerno, and G. V. Rinati, Phys. Rev. B **58**, 12377 (1998).
[10] M. Salerno and M. R. Samuelsen, Phys. Rev. B **59**, 14653 (1999).
[11] U. Mortensen, M. Salerno, and M. R. Samuelsen, Phys. Lett. A **285**, 350 (2001).
[12] M. Salerno, M. Samuelsen, and A. Yulin, Phys. Rev. Lett. **86**, 5397 (2001).
[13] A. L. Pankratov, Phys. Rev. B **65**, 054504 (2002).
[14] A. L. Pankratov, Phys. Rev. B **66**, 134526 (2002).
[15] V. P. Koshelets, S. V. Shitov, P. N. Dmitriev, A. B. Ermakov, L. V. Filippenko, V. V. Khodos, V. L. Vaks, A. M. Baryshev, P. R. Wesselius, and J. Mygind, Physica C **367**, 249 (2002).
[16] V. P. Koshelets, P. N. Dmitriev, A. S. Sobolev, V. V. Khodos, A. L. Pankratov, V. L. Vaks, A. M. Baryshev, P. R. Wesselius, and J. Mygind, Physica C **372–376**, 316 (2002).
[17] S. V. Shitov, V. P. Koshelets, A. B. Ermakov, P. N. Dmitriev, L. V. Filippenko, V. V. Khodos, V. L. Vaks, P. A. Yagoubov, W.-J. Vreeling, and P. R. Wesselius, IEEE Trans. Appl. Supercond. **13**, 684 (2003).
[18] V. P. Koshelets, S. V. Shitov, A. B. Ermakov, L. V. Filippenko, O. V. Koryukin, A. V. Khudchenko, M. Yu. Torgashin, P. Yagoubov, R. Hoogeveen, and O. M. Pylypenko, IEEE Trans. Appl. Supercond. **15**, 960 (2005).
[19] V. P. Koshelets, P. N. Dmitriev, A. B. Ermakov, A. S. Sobolev, M. Yu. Torgashin, V. V. Kurin, A. L. Pankratov, and J. Mygind, IEEE Trans. Appl. Supercond. **15**, 964 (2005).
[20] J. Mygind, V. P. Koshelets, M. Samuelsen, and A. S. Sobolev, IEEE Trans. Appl. Supercond. **15**, 968 (2005).
[21] E. Goldobin, A. Sterck, and D. Koelle, Phys. Rev. E **63**, 031111 (2001).
[22] M. R. Samuelsen and S. A. Vasenko, J. Appl. Phys. **57**, 110 (1985).
[23] Y. Zhang, Ph.D. thesis, Chalmers University of Technology, 1991.
[24] J. R. Tucker and M. J. Feldman, Rev. Mod. Phys. **57**, 1055 (1985).
[25] K. K. Likharev, *Dynamics of Josephson Junctions and Circuits* (Gordon and Breach, New York, 1986).